Published in final edited form as:
Neuroscience. 2011 June 30; 185: 14–26. doi:10.1016/j.neuroscience.2011.04.015.

Up-regulation of Tetrodotoxin-Sensitive Sodium Currents by Prostaglandin E_2 in Type-4 Rat Dorsal Root Ganglion Cells

Pradeep K. Tripathi, **Carla G. Cardenas**, **Carlos A. Cardenas**, and **Reese S. Scroggs**
Department of Anatomy and Neurobiology, University of Tennessee Health Science Center, Memphis, Tennessee 38163

Abstract

Mechanisms were studied by which prostaglandin E_2 (PGE_2) up-regulates Na^+ currents (I_{Na}) in medium diameter dorsal root ganglion (DRG) cells that express large T-type Ca^{2+} currents (type-4 DRG cells). PGE_2 or the adenylyl cyclase (AC) activator forskolin (10 μM) up-regulated peak I_{Na} evoked by test potentials (TP) to −10 mV by an average of 13.5% and 21.8%, respectively. The PGE_2 and forskolin induced up-regulation of I_{Na}, evoked with TPs to −10 mV, began approximately 15–20 sec after initiation of drug exposure and continued gradually over the course of 2–3 min. Both PGE_2 and forskolin significantly increased peak conductance without significantly shifting the voltage at which I_{Na} was ½ activated (V_a) or ½ steady state inactivated. However, although V_a was not significantly shifted, both PGE_2 and forskolin induced a proportionally greater percent increase in conductance at weak TPs to around −30 mV compared to stronger TPs to around 10 mV. The PGE_2 induced up-regulation of I_{Na} was occluded by prior up-regulation with forskolin, and the up-regulation of I_{NA} by both PGE_2 and forskolin was blocked by the protein kinase A (PKA) antagonist Rp-cAMPs and 50 nM tetrodotoxin (TTX). In the presence of Rp-cAMPs, both PGE_2 and forskolin induced decreases in I_{Na} that peaked around 25 sec following initiation of PGE_2/forskolin application. The decrease induced by PGE_2 averaged 8.5%, which was significantly greater than the average 3.5% decrease induced by forskolin. Estimation of kinetic rate constants by fitting I_{Na} with a Markov channel state model, suggested that both PGE_2 and forskolin up-regulated I_{Na} by changing channel gating rather than by increasing channel number or unitary conductance. The data suggest that application of PGE_2 may initially induce a relatively rapid down-regulation of TTX-sensitive I_{Na} (signaling pathway uncharacterized), followed by a gradual up-regulation of I_{Na} via activation of an AC/PKA-dependent signaling pathway. The up-regulation of I_{Na} in sensory neurons with type-4 cell bodies may increase excitability and strengthen signaling, and may play some role in the allodynia and hyperalgesia associated with injury to nerves and peripheral tissues.

Keywords

Inflammatory mediator; T-type Ca^{2+} current; TTX-sensitive Na^+ current; Low-threshold mechanoreceptor; D-hair receptor; Sensitization

Corresponding Author: Reese Scroggs, University of Tennessee Health Science Center, Department of Anatomy and Neurobiology, 855 Monroe Avenue, Memphis, TN, 38163 Tel: (901) 448-7470; Fax: (901) 448-9173; rscroggs@uthsc.edu.

Medium diameter DRG cells that exhibit very large T-type Ca^{2+} currents have been the focus of several studies (Abdula and Smith, 1997; Cardenas et al., 1995, 1997; 1999; Coste et al., 2007; Dubreuil et al., 2004; Petruska et al., 2000, 2002; Scroggs and Fox, 1992ab; Scroggs et al., 1994; Shin et al., 2003; White, 1990; White et al., 1989). An apparently analogous subgroup of DRG cells were classified as type-4 DRG cells by Cardenas et al. (1995) based on soma diameter (average ≈ 35 μM), expression of large T-type Ca^{2+} currents and large I_H currents, and insensitivity to capsaicin. Studies in several laboratories suggest that type-4 DRG cells express a curious mixture of characteristics; some typically associated with nociceptive afferents, and others typically associated with non-nociceptive afferents. Two studies employing molecular biology and electrophysiology techniques led to the hypothesis that a subpopulation of mouse DRG cells with medium diameters and large T-type Ca^{2+} currents (similar to type-4 DRG cells), are somata of D-hair receptors (Dubreuil et al., 2004; Shin et al., 2003). Also, Coste et al. (2007) described a subpopulation of cultured medium diameter rat DRG cells with large T-type Ca^{2+} currents, which exhibited low-threshold mechanosensitivity consistent with D-hair receptors. However, it has never been directly confirmed that medium diameter DRG cells with large T-type Ca^{2+} currents are the somata of D-hair receptors, using appropriate stimuli in an intact preparation.

On the other hand, another study reported several nociceptor-like characteristics (ATP-generated currents, proton activated currents, and long duration afterhyperpolarizations) in DRG cells categorized as type-4 using the Cardenas et al. (1995) criteria (Fang et al., 1995; Petruska et al., 2000). In addition we have shown that Na^+ currents and I_H currents in type-4 DRG cells are up-regulated by PGE_2 and serotonin, respectively (Cardenas et al., 1997, 1999). Sensitivity to inflammatory mediators is a typical characteristic of nociceptors. In any case, the sensitivity of type-4 DRG cells to inflammatory mediators and acidity suggest that, whatever modality is served by the corresponding sensory neurons, it is probably subject to modulation by inflammation. Continued characterization of type-4 DRG cells and the modality of the sensory neurons they represent may eventually unravel a novel and important story in sensory physiology.

As alluded to above, we previously reported that the Na^+ currents expressed by type-4 DRG cells are up-regulated by PGE_2 (Cardenas et al., 1997). This is unusual because, under control conditions, the Na^+ current expressed by type-4 DRG cells is predominately mediated by tetrodotoxin-sensitive (TTX-s) channels, which are generally down-regulated when phosphorylated via activation of protein kinase A (PKA) or protein kinase C dependent signaling pathways (Cantrell et al., 1996, 1997; Cardenas et al., 1997; Li et al., 1992). However, there are other reports of TTX-s channel up-regulation in sensory neurons in response to activation of PKA (Docherty and Farrag, 2006), and neuronal injury and inflammation (Abdulla and Smith, 2001; Black et al., 2004). The present study expands our earlier findings by including experiments on the TTX-sensitivity of the PGE_2 up-regulated current, the effects of PGE_2 on the voltage-dependence of activation and steady state inactivation of the Na^+ current, and involvement of an adenylyl cyclase/protein kinase A-dependent signaling pathway in the up-regulation of the Na^+ current by PGE_2. Finally, the current records are fitted with a Markov channel state model for the purpose of determining possible changes in channel gating that could be involved

Experimental Procedures

Preparation of DRG Cells

All procedures involving animals were approved the University of Tennessee Health Science Center Animal Use and Care Committee, and carried out in accordance with the National Institute of Health Guide for the Care and Use of Laboratory Animals. Male rats (50–100g), Sprague Dawley (purchased from Harlan) were rendered unconscious with

Isoflurane, decapitated, and dorsal root ganglia (DRG) from lumbar and thoracic regions dissected out. DRG were incubated at 34° C for 1/2 hour in Tyrodes' solution (composition below) containing 2 mg/ml collagenase type 1A and 2 mg/ml protease (Sigma-Aldrich). Following enzyme treatment the enzymes were washed away from the DRG, and the DRG were stored at room temperature in artificial cerebral spinal solution containing (in mM) 124 NaCl, 3.5 KCl, 1.2 KH_2PO_4, 26 $NaHCO_3$, 1 $MgSO_4$, 2.4 $CaCl_2$, and 10 glucose, and continuously bubbled with 95% O_2/5% CO_2, pH 7.3. DRG harvested on a given day were used within 8 hours following harvest. Immediately prior to whole-cell patch-clamp experiments, 3–4 ganglia were selected, and individual DRG cell bodies were dispersed by trituration in Tyrode's solution containing (in mM); 140 NaCl, 4 KCl, 2 $MgCl_2$, 2 $CaCl_2$, 10 glucose, 10 HEPES, pH 7.4 with NaOH. An aliquot of suspended DRG cells was immediately transferred to a plastic 35-mm petri dish, where many settled and adhered to the bottom within 5 minutes. Non-adhered cells were washed away and adhered cells were superfused with Tyrodes' solution. Whole-cell patch-clamp experiments were carried out at room temperature within about 1 hour after the DRG cells were plated out into the 35-mm petri dish, which served as the recording chamber. DRG cells used in these experiments were never exposed to culture conditions or nerve growth factor after removal from the rat.

Data Acquisition

Experiments were restricted to medium diameter DRG cells (average diameter ≈ 35 μm). Each DRG cell included in the study was characterized as type-4 based on soma diameter, expression of prominent I_H current, and rapidly activating and inactivating Na^+ currents (Fig 1A and B). Previous studies have shown that these characteristics reliably predict the large T-type Ca^{2+} currents (Cardenas et al., 1995, 1999).

Data acquisition and analysis were accomplished with P-Clamp 8.2, using an Axopatch 200A/B amplifier coupled with a Digidata A-D/D-A converter (Axon Instruments). Data were leak subtracted using the P/4 method. Patch electrodes were coated with Sylgard to about 200 μm from the tip, and fire polished to a resistance of 0.8–2.0 MΩ. The electrodes were filled with a solution containing (in mM); 120 CsCl, 5 2Na-ATP, 0.4 2Li-GTP, 5 $MgCl_2$, 5 EGTA, 1.86 $CaCl_2$, 20 HEPES, adjusted to pH 7.4 with CsOH. (Total $[Ca^{2+}]_i$ was calculated to be 100 nM. The patch clamp amplifier was tuned to compensate for series resistance (R_s) without nulling the whole-cell capacitance.

Solutions were changed around the cell under study by means of a small glass capillary tube placed near the cell in the bath, as described earlier (Cardenas et al., 1997). The external solution used for isolation of Na^+ currents contained (in mM): 50 NaCl, 100 TEA, 2 $CaCl_2$, 5 $MgCl_2$, 10 HEPES, 0.5 $CdCl_2$, pH 7.4 with TEA-OH. In this solution, the tail currents exhibited a prominent slow component ($\tau \approx 1.5$ ms, see Fig. 1A). This slow component is consistent with the deactivation of T-type Ca^{2+} channels (Nelson et al., 2010), and probably represents reversal of the block of T-type Ca^{2+} channels by Cd^{2+} as the membrane potential returned to the negative holding potential (Carbone and Swandulla, 1989). Chemicals and salts used to make up the external and pipette solutions were obtained from Sigma-Aldrich.

Data Analysis

For estimation of the voltage where the Na^+ current was ½ activated (V_a) plots of normalized conductance versus voltage (G-V) were derived from data acquired regarding current amplitude versus voltage (I-V), and fitted with a Boltzmann function of the form: $1/(1+\exp((V_a - V_{test})/k))$, where V_{Iest} = test potential and k = slope. I-Vs and G-Vs were adjusted for the effects of series resistance (R_s) on test potential (TP). Series resistance (R_s) was calculated from capacity transients recorded from each DRG cell after R_s compensation and averaged 0.88 ± 0.06 MΩ for the first I-V, and 1.07 ± 0.08 MΩ for the second I-V, in

the 17 DRG cells included in experiments on I-V and G-V relationships. The calculated R_s values were used to determine TP error (V_{error}) using the formula $V_{error} = R_s * I$. Current amplitudes were adjusted to account for rundown based on the rate of change in the amplitude of control currents recorded from each cell prior to drug application, using the method described in Scroggs and Fox (1992).

Correction of I-V Data for Spontaneous Drift

I-Vs and the estimations for V_a were also corrected for spontaneous drift caused by dialysis of the cell interior, based on recordings from 4 untreated control type-4 DRG cells. I-V data was acquired from the 4 untreated control cells before and after an average recording period of 213 ± 6 sec, which corresponded closely to the time between acquisition of pairs of I-Vs from the PGE_2 and forskolin treated DRG cells. Currents were evoked by TPs to −10 mV every 5 sec in between I-Vs to mimic the drug treatment paradigm. For all DRG cells included in experiments on current activation (untreated controls before and after 213 sec, control and PGE_2 treated, and control and forskolin treated) the current amplitudes corresponding to the original command voltages (−55, −50, −45, −40, −35… +30) were extrapolated graphically from individual I-Vs. The purpose of this procedure was to eliminate differences in current amplitude resulting from the effects of R_s on TP. Then the second set of each pair of extrapolated untreated control currents was scaled in amplitude so that the currents corresponding to a TP to −10 mV matched those of the first set at their peaks to correct for rundown. The value of −10 was chosen because this was closest to the TP employed to monitor current amplitude versus time and to adjust current amplitude for rundown in the PGE_2 and forskolin experiments. A set of correction factors was calculated for each pair of untreated control DRG cells by dividing the first set of current amplitudes by the second set of current amplitudes for each TP (Fig 2C). Multiplying the second set of current amplitudes by the correction factors yielded the first set of current amplitudes. The four sets of correction factors were averaged to arrive at a final set of correction factors (Fig. 2C). To correct each I-V acquired following PGE_2 or forskolin treatment, each individual set of current amplitudes corresponding to each TP was multiplied by the corresponding averaged correction factors.

The voltage-dependency of steady state inactivation was analyzed in type-4 DRG cells before and after treatment with 10 μM PGE_2 or forskolin. The DRG cells were held at −80 mV for 5 sec and given 500 ms conditioning potentials to −100 mV through −20 mV, each followed by a TP to −10 mV to assess the level of inactivation. Normalized plots of I/Imax were fitted with the Boltzmann function: $1/(1+exp((V_h-V_{condition})/k))$, where V_h was the voltage where the current was ½ inactivated and $V_{condition}$ was the voltage of the 500 ms conditioning pulse.

Model Fitting

A Markov channel state model was fitted to sets of Na^+ current records using similar methods as those described previously (Nelson et al., 2010). Sets of currents evoked by TPs ranging from −40 mV to −5 mV, acquired before and after PGE_2 treatment (n = 7) before and after forskolin treatment (n = 6) and from untreated controls before and after an average 213 seconds of continuous recording (n = 4), were used for fitting. The delay between the onset of the TP and the beginning of current activation was reduced to 20 μs to facilitate the fit of a model with three resting states (Fig 6A). The first 221 data points (50 kHz sampling rate) of the thus edited currents were used for fitting to increase the rate of iteration.

A model (Fig. 6A) was chosen based on trial and error, and was the simplest that could provide an accurate fit to the data. The main purpose of the modeling was to provide realistic simulations of current shape at equivalent voltages, thus goodness of fit was

emphasized over the model's ability to represent all aspects of channel gating. Consequently, the model does not represent channel availability at different membrane potentials nor recovery from inactivation. Details regarding which parameters are set free, scaled, or fixed are provided in the legend to Fig. 6.

The model was represented mathematically and fitted to the current records using the MAC algorithm in the QuB software suite (Milescu et al., 2005), which can be downloaded at no cost from www.qub.buffalo.edu. For each data point in a given current record, the fitting algorithm was provided with the value of the TP, corrected for R_S (Fig 6C). To calculate whole cell current amplitude at different voltages, the MAC algorithm requires input regarding unitary conductance, reversal potential, and the number of available channels. TTX-sensitive Na^+ channel unitary current amplitude at −10 mV in the presence of 50 mM external Na^+ was estimated at −0.33 pA, based on single channel recordings from medium diameter DRG cells in 250 mM external Na^+ (Cardenas and Scroggs, 2003), and a study (Barber et al., 1991) showing that unitary current amplitude decreased ≈ 78% for $Na_V1.5$ channels when the external Na^+ concentration was decreased from 250 mM to 50 mM. The number of channels corresponding to whole-cell Na^+ currents evoked by TPs to −10 mV was estimated according to the formula: I ÷ −0.33 ÷ 0.32 ÷ Gn, where (*I*) is the peak current amplitude evoked by a TP to −10 mV (extrapolated graphically), (*0.32*) is the maximum open probability observed for TTX-sensitive Na^+ channels in squid axon (Patlak, 1991) and (*Gn*) is the normalized conductance observed for TPs to −10 mV. The calculated number of channels per DRG cell averaged 88,720 ± 13,190. The unitary current amplitudes (*i*) corresponding to currents evoked by other TPs was calculated by a re-arrangement of the above formula; *i = I* ÷ (*channel number * 0.32 * Gn*). Unitary conductance (*g*) was estimated by linear regression of *i vs V*, and averaged 6.91 ± 0.16 pS. The calculated relationship of *i* versus voltage was linear over the range of TPs used to evoke currents for fitting. Thus an ohmic model ($i = g*(V - V_r)$, was employed in MAC to calculate *i* at different voltages. The reversal potential (V_r) for each data set was estimated by linear regression of current amplitude versus voltage over TPs to 20 mV, 25 mV, and 30 mV (corrected for R_s), using the formula; I = mV*a + b, and V_r was calculated as −b ÷ a. Rate constants (*k*) were calculated in MAC based on the voltage record that accompanied each current, using the equation: $k = k_0 \times exp(k_1 \times V)$, where *k* is the rate constant [s^{-1}] at a given voltage *V*, and k_0 [s^{-1}] is the rate constant at zero potential. For convenience, the voltage was expressed in mV. The exponential factor k_1 [mV^{-1}] is equal to $z\delta e/k_B T$, where *z* = the valence of the gating charge moved over a fraction δ of the electric field, *e* = the charge of an electron, k_B is Boltzmann's constant, and *T* is the absolute temperature. When reporting the degree of voltage-dependence in the results, the values of k_1 are written as shown in MAC (i.e., 0.01, 0.06). Larger absolute values correspond to a greater degree of voltage-dependence (Milescu et al., 2005).

Goodness of fit of a given model to a current record was assessed via a direct comparison of the current amplitude versus time predicted by the model (given a set of parameters) to the real current amplitude versus time. Discrepancies between the real and predicted currents were quantified as the unweighted sum of squares according to the formula: sum of squares = $\Sigma(I_t - \mu_t)^2$, where I_t = real current amplitude at a given time point, and μ_t = the isochronal predicted current amplitude. The optimizer employed in MAC used the sum of squares as criterion to search for optimum values for the free parameters (Milescu et al., 2005). The best fit was defined as the set of parameters last estimated before successive iterations failed to further minimize the sum of squares. Strategies employed to avoid local minima and detect multiple solutions included starting fits with different seed values, and restarting fits following perturbation of selected optimized values. Regarding the parameter values reported, no alternate solutions were detected where the sum of squares was minimized to a similar degree.

Statistics

The data are expressed as the mean ± the standard error of the mean. Statistical analyses were preformed using Systat (SPSS Inc.). Statistical analyses of putative differences between groups of paired data were carried out with the non-parametric Wilcoxon test. The non-parametric Mann-Whitney U-test was utilized to assess the significance of differences between two groups of independent data, and the non-parametric Friedman test was used to assess the significance of change of a single variable over a series of TPs. In one set of comparisons (see Fig. 5C) some of the groups were used in multiple comparisons. In these cases the α-level was adjusted according to the number of multiple comparisons using the Bonferroni method.

Results

Effects of PGE_2 on Na^+ Current Activation

In 7 type-4 DRG cells held at −60 or −70 mV and given TPs to −10 mV, application of 10 μM PGE_2 increased peak Na^+ current by an average of 15% ± 4% over a period of 2 minutes (Fig. 2A). The increase in Na^+ current amplitude began approximately 30 seconds following initiation of PGE_2 application (Fig 2A). Figure 2A also shows current amplitude versus time for Na^+ currents recorded from 4 untreated control type-4 DRG cells. Over the same time period during which PGE_2 was tested, untreated control current amplitude ran down approximately 7% on average, suggesting that the apparent increase in current amplitude observed following application of PGE_2 was not due to spontaneous current run up.

In the above mentioned 7 PGE_2 treated DRG cells, the effects of PGE_2 on Na^+ currents evoked by a family of TPs (I-V) was analyzed. Averaged records from the 7 DRG cells corresponding to currents evoked before and after PGE_2 treatment by TPs (uncorrected) from −35 mV to −10 mV are depicted in Fig 2B. Inspection of pairs of I-Vs acquired from individual untreated controls at different times (see Experimental Procedures), indicated that some of the changes in current amplitude occurring during the course of the PGE_2 experiments was due to spontaneous drift. The pairs of untreated control currents were scaled so that currents evoked by TPs to −10 mV were equivalent at their peaks. The TP to −10 was chosen because this was the same TP used to monitor and adjust currents for rundown in the PGE_2 and forskolin experiments. Given this adjustment, currents evoked by TPs negative to −10 mV tended to increase with time while currents evoked by TPs more positive than −10 mV tended to decrease slightly with time. Thus, the PGE_2 I-V data was corrected using a set of correction factors derived from the untreated control data (Fig 2C, see Experimental Procedures). Corrected I-V and G-V data are depicted in Fig 2D and E. According with the uncorrected data PGE_2 shifted the V_a by an average of −1.9 ± 0.6 mV, while after correction the shift was −0.4 ± 0.7 mV. A significant effect of PGE_2 on V_a was not detected for the corrected data. The slope (k) of the corrected I-V curves averaged 8.1 ± 0.1 under control conditions and 8.0 ± 0.1 after PGE treatment, which was also not significantly different. However, PGE_2 treatment did significantly increase peak conductance from a control value of 257 ± 52 nS to 291 ± 55 nS ($p < 0.05$, Wilcoxon test).

Inspection of the averaged current records shown in Fig 2B suggests that PGE_2 induced a larger proportional increase in current amplitude for currents evoked with more negative TPs versus stronger TPs. However, these visual comparisons are obscured by the fact that, due to the effects of R_s on TP, the peaks of the larger currents recorded following PGE_2 treatment were acquired at more positive voltages than the smaller control peaks. However, analysis of the corrected G-V data demonstrated that there was a significant change in the percent increase in conductance following PGE_2 treatment over a range of TPs (uncorrected)

from −30 mV to +30 mV (Fig. 2F, Friedman's test, $p < 0.05$). The peak percent increase in conductance, observed at ≈−20 mV, was significantly greater than that observed at ≈0 mV ($p < 0.05$, Wilcoxon test).

Effects of Forskolin on Na^+ Current Activation

In 6 type-4 DRG cells (different from those tested with PGE_2) held at −60 or −70 mV, application of 10 μM forskolin increased peak Na^+ current by an average of 25% ± 4% over a period of 2 minutes (Fig. 3A). The time course of the increase in current amplitude induced by forskolin was similar in time-course to that induced by treatment with PGE_2. Experiments with Rp-cAMPs (below) suggest that the forskolin effect was mediated by an increase in adenylyl cyclase activity.

The effects of forskolin on I-V data was also tested on the above mentioned 6 DRG cells. The averaged currents from these cells corresponding to TPs (uncorrected) to −35 mV through −5 mV are shown in Fig 3B. The I-V data was corrected using the same method employed for PGE_2, and the corrected I-V and G-V data are shown in Fig 3C and D. According with the uncorrected data, V_a was shifted by an average of −3.3 ± 0.8 mV, while following correction the shift averaged −1.8 ± 0.7 mV. The corrected shift was not statistically significant. Also, the slope of the corrected I-V curves before (7.7 ± 0.4) and after (7.6 ± 0.4) forskolin treatment was not significantly changed. However, forskolin significantly increased peak conductance from an average control value of 134 ± 15 nS to 163 ± 16 nS ($p < 0.05$, Wilcoxon test).

Similar to the case regarding PGE_2, inspection of the averaged current records depicted in Fig 3B suggest that forskolin induced a larger proportional increase in current amplitude for currents evoked with weak TPs versus strong TPs. This was supported by analysis of the corrected G-V data shown in Fig 3D, which indicated a significant change in percent increase in conductance by forskolin over TPs ranging from −50 mV through +30 mV (Fig. 3E, Friedman test, $p < 0.05$). The peak percent increase in conductance, observed at ≈−50 mV, was significantly larger than that observed at ≈0 mV ($p < 0.05$, Wilcoxon test). Furthermore, the difference between the peak increase in conductance and that observed at ≈0 mV for forskolin was significantly greater than the analogous difference regarding PGE_2 ($p < 0.05$, Mann-Whitney U-test).

Effects of PGE_2 and Forskolin on Steady State Inactivation

Whether or not the PGE_2 induced increase in Na^+ current amplitude was associated with a change in steady state inactivation was tested in 5 type-4 DRG cells, using 500 ms conditioning potentials to −100 mV through −20 mV. In these cells, 10 μM PGE_2 increased Na^+ currents evoked by a TP to −10 mV by an average of 11.9 ± 2.8%. The voltage at which the current was ½ inactivated (V_h) averaged −58.8 ± 0.6 mV under control conditions, and −60.0 ± 0.7 mV following treatment with 10 μM PGE_2, which was not significant (Fig. 4AB). In one type-4 DRG cell, where forskolin increased current amplitude by 12.8%, V_h was little affected (data not shown, control V_h = −56.9 mV, forskolin V_h = −57.8 mV).

Occlusion of PGE_2 by Forskolin

To test for occlusion, 10 μM PGE_2 was applied following a maximal increase in current amplitude induced by 10 μM forskolin. In the 5 type-4 DRG cells included, forskolin increased current amplitude by 19.4 ± 2.2%. Subsequent application of PGE_2 in the continued presence of forskolin did not significantly increase the current amplitude (Fig. 5A and C). Application of 50 nM TTX following treatment with forskolin and PGE_2 nearly completely blocked the inward current (Fig. 5A inset). The small inward current remaining

following treatment with TTX was slowly activating, and was negligible at the point in time where the peak of the TTX-sensitive current occurred (Fig. 5A inset).

Blockade of PGE_2 and Forskolin Up-regulation by Rp-cAMPs

The possible involvement of protein kinase A (PKA) in the up-regulation of TTX-s Na^+ current by PGE_2 and forskolin was tested by observing the effects of either agent with the selective PKA antagonist Rp-cAMPs (100 μM) included in the pipette solution. As shown in Fig. 5 B and C, inclusion of Rp-cAMPs in the pipette solution produced a strong block of PGE_2 and forskolin induced up-regulation of TTX-s Na^+ currents, when current amplitude was assessed at 115 sec following initiation of drug treatment. The time point of 115 sec corresponds to times following initiation of drug treatment in Figs. 2A, 3A, 4A, and 5A where increases in TTX-s current amplitude produced by PGE_2 and forskolin in the absence of Rp-cAMPs were assessed. Overall, in the absence of Rp-cAMPs, PGE_2 ($n = 12$) increased TTX-s current by an average of 13.5 ± 2.5%, which was significantly less than the 21.8 ± 2.4% increase produced by forskolin ($n = 12$) under the same conditions ($p < 0.05$, Mann Whitney U-test). At the same 115 sec time point with 100 μM Rp-cAMPs in the pipette, the change in TTX-s current amplitude was significantly reduced to an average of 3.0 ± 2.3% for forskolin ($n = 10$, $p < 0.05$, Mann-Whitney U-test), and −6.2 ± 3.6% for PGE_2 ($n = 7$, $p < 0.05$, Mann Whitney Utest, Fig. 5B and C).

Interestingly, with Rp-cAMPs in the pipette, both forskolin and PGE_2 treatment produced a relatively rapid decrease in TTX-s currents, which was significantly greater for PGE_2 (−8.5 ± 1.9% $n = 7$) compared to forskolin (−3.5 ± 0.9%, $n = 10$, $p < 0.05$, Mann-Whitney U-test, Fig. 5B and C). The peak decrease in TTX-s current amplitude occurred at an average time following initiation of drug treatment of 25.5 ± 2.8 sec for forskolin and 26.4 ± 4.5 sec for PGE_2 (Fig 5B and C, time point rounded off to 25 ms). Occasionally, we observed biphasic responses to PGE_2 ($n = 4$) and forskolin ($n = 3$) applied in the absence of Rp-cAMPs, where the TTX-s current first decreased and then increased. An example regarding PGE_2 is shown in Fig. 5D.

Model Fitting

Initially, the Markov channel state model shown in Fig 6A was fitted to real untreated control I-V records acquired before and after 213 sec (4 pairs), real control and PGE_2 treated I-V records (7 pairs), and real control and forskolin treated I-V records (6 pairs). In each case, the records selected were evoked by voltage commands from −40 mV to −5 mV. Fig. 6B shows fits of the model to the averaged real control and PGE_2 records, and demonstrates that the model could fit the records closely. Similar good fits were observed for the individual data sets. The effects of R_s on TP were taken into account by encoding the appropriate changes into the voltage file (Fig 6C), which is used by MAC to fit the model to the data (see Experimental Procedures). Fig 6D shows selected rate constants estimated by MAC during individual fits of the model to sets of real control records acquired before PGE_2 (control 1) or forskolin treatment (control 2). However, the rate constants corresponding to PGE_2 and forskolin treatment were obtained by fitting simulated records corrected for changes in channel gating observed in the untreated control DRG cells over time. The corrected simulated PGE_2 treatment records, and the records used for correction are shown in Fig. 7B and A, respectively. The methods used for simulation and correction are described below.

The results of the model fitting suggest that PGE_2 induced a significant increase in transition rates from resting to open (KC3O) and from the second inactivation state to the third inactivation state (kI2I3), and a significant decrease in the voltage-dependence term (VdBack) corresponding to backwards transitions through the resting states. In contrast, the

results suggest that forskolin induced a significant increase in forward transitions through the resting states (kC1C2/kC2C3) as well as kC3O, and a significant decrease in inactivation from the closed state (kC1I1). Thus the modeling suggests that PGE_2 and forskolin differed regarding their effects on kC1C2/kC2C3, kC1I1, kI2I3 and VdBack, but had a similar effect on kC3O.

Simulations of the effect of changing rate constants one at a time indicate that increases in kC1C2/kC2C3, and kCO3 would increase peak amplitude of currents evoked by TP−30 mV, while an increase in VDBack, would decrease peak current (Fig. 6E, F, and G). Similar magnitude changes in kC1I1, and kI2I3, mainly affect amplitude over the last 1/3 of the current (data not shown).

PGE_2 and Forskolin Induced Changes in Macroscopic Current Activation and Inactivation Rates

The modeling study was extended to see how the PGE_2 and forskolin induced modulation of channel gating translated into changes in macroscopic activation and inactivation rates. Paired control and drug treatment records were simulated at equivalent voltages so that they could be directly compared in analyses of possible changes in these parameters. Such comparisons were not possible with the real currents because control and drug treated currents were acquired at different voltages, due to the effect of R_s on TP.

For correction of the real currents corresponding to PGE_2 and forskolin treatment for spontaneous drift in channel gating, current records corresponding to each of the 7 PGE_2 data sets, 6 forskolin data sets, and 4 untreated control data sets were simulated, using versions of the model endowed with the appropriate sets of parameters generated during fitting of the real currents. A set of correction sweeps was generated by subtracting the second set of untreated control records from the first (for each pair of untreated control I-Vs), and then averaging the 4 sets of difference records. The set of correction sweeps obtained by this procedure is illustrated in Fig 7A. Before subtraction, the correction sweeps were scaled up or down to adjust for differences regarding the amplitudes of the simulations of currents evoked by TP −10 mV. The averages of the simulations corresponding to control PGE_2 treatment (the latter corrected), are shown in Fig 7B. (Note that the individual corrected PGE_2 treatment simulations, averaged in Fig. 7B, and analogous corrected forskolin treatment simulations were used for generation of rate constants corresponding to drug treatment in the modeling study shown in Fig.6).

One approach taken to determine whether PGE_2 produced changes in channel gating was to subtract the control simulations from the PGE_2 treatment simulations, after the former were scaled to equal the latter at their peaks. This resulted in a set of subtraction currents that were distinctly different than those obtained by subtraction of untreated control records (compare Fig 7A and C). Also, the subtraction records were obviously different from those generated by subtraction of similarly scaled simulated records, where the amplitude was initially increased by simulating increased channel number or increased unitary conductance (Fig 7D, E, and F). In these latter cases the subtraction records are perfectly straight lines (Fig 7F).

Another approach was to analyze the simulations of currents evoked by TP −5 mV (Fig. 7B) regarding macroscopic inactivation rate, time to peak, and the current amplitude at the end of each record for simulations scaled to be equal at their peaks. Similar to the real currents, the macroscopic inactivation of the simulated currents was best fit by a double exponential function. Both PGE_2 and forskolin decreased the fast and slow time constants of inactivation, and significantly increased the amount of the fit of the double exponential function corresponding to the slow time constant ($p < 0.05$, Wilcoxon test, $n = 7$ for PGE_2

and 6 for forskolin). Also, both PGE_2 and forskolin decreased the amplitude of the current remaining at the end of the sweep, when the peaks of the currents were scaled to be equal ($p < 0.05$, Wilcoxon test). Finally, forskolin, but not PGE_2, produced a significant decrease in time to peak current ($p < 0.05$ for forskolin, Wilcoxon test).

Discussion

The main contribution of this work is the demonstration that PGE_2 up-regulates a TTX-sensitive Na^+ current expressed by type-4 DRG cells, and that this process involves activation of a cAMP/PKA cascade and changes in channel gating behavior. We previously reported that PGE_2 up-regulated Na^+ currents in type-4 DRG cells (Cardenas et al., 1997), but the TTX-sensitivity of the up-regulated current, the second messenger system involved, and the underlying mechanism was not investigated in that prior publication. In the present study, we demonstrated that the inward current was almost entirely blocked by TTX, following maximal up-regulation of the current by application of forskolin + PGE_2, suggesting that up-regulation of a TTX-resistant Na^+ current could not account for the data. There was a very small amount of inward current that was resistant to TTX. However, this current was slowly activating and nominally 0 at the peak of the TTX-s Na^+ current where the up-regulation occurred.

The observation that up-regulation of the TTX-s Na^+ current by both PGE_2 and forskolin was blocked by the PKA antagonist Rp-cAMPs, and that forskolin occluded the effects of PGE_2 on current amplitude suggests that both agents targeted the TTX-sensitive Na^+ current, via a PKA-dependent signaling pathway. Up-regulation of TTX-s Na^+ channels in rat DRG cells via a PKA-dependent signaling pathway has been previously reported (Docherty and Farrag, 2006). However, in that study no attempt was made to see whether inflammatory mediators could up-regulate TTX-s channels via the same pathway. As mentioned by Docherty and Farrag (2006), it seems unlikely that the TTX-s current in DRG cells is up-regulated due to phosphorylation of PKA consensus sites on the channel, as that has been shown to result in a decrease in current amplitude (Li et al., 1992; Smith and Goldin, 2000). Smith and Goldin (2000) provided evidence (in frog oocytes) that PKA phosphorylates an accessory protein that then somehow up-regulates the TTX-s Na^+ current via an interaction with the I–II linker.

In the present study, we observed that PGE_2, and to a lesser degree forskolin, down-regulated TTX-s Na^+ currents when applied to type-4 DRG cells perfused with Rp-cAMPs internally. The relatively rapid time course of the down-regulation is consistent with the time course of down-regulation of TTX-s Na^+ currents in central neurons produced by phosphorylation of consensus sites on the corresponding channels via activation of PKA- or PKC-dependent pathways (Cantrell et al., 1996, 1997). Also, the observation that PGE_2 induced down-regulation was significantly greater than forskolin induced down-regulation may explain why forskolin produced a significantly greater up-regulation of TTX-s Na^+ currents than PGE_2. “Correcting” the average up-regulation observed for PGE_2 and forskolin in the presence of Rp-cAMPs for the respective down-regulation observed for each in the absence of Rp-cAMPs, cancels out the significant difference between the two regarding up-regulation. Thus, it seems possible that the down-regulation directly opposes the up-regulation observed for forskolin and PGE_2.

In any case, the observation in this study that the down-regulation occurred in the presence of Rp-cAMPs suggests that the down-regulation may occur via some signaling pathway that is not dependent on PKA. A PKC-dependent pathway is one possibility in the case of PGE_2, since PGE_2 receptors have been shown to couple to PKC, and PKC-dependent pathways have been shown to couple negatively to TTX-s Na^+ channels (Cantrell et al., 1996; Gold et

al., 1998; Bley et al., 1998). However, it is difficult to understand how forskolin produced down-regulation, since forskolin has not been shown to activate PKC or other non-adenylyl cyclase dependent signaling pathways. It is possible that the down-regulation of TTX-s current by forskolin is a non-specific effect, which coincidentally has a similar time course as the down-regulation induced by PGE_2. We observed that di-deoxyforskolin (often used as a control for non-specific effects of forskolin), blocked TTX-s currents in type-4 DRG cells. Subsequently, use of di-deoxyforskolin was abandoned as a control in our experiments.

In several type-4 DRG cells tested with PGE_2 in the absence of Rp-cAMPs, we observed that PGE_2 application produced a small decrease in TTX-s Na^+ current amplitude that preceded the beginning of the overall increase. Possibly the intermittence of down-regulation by PGE_2 in the absence of Rp-cAMPs could have been due to an obscuring of the down-regulation by the up-regulation. In any case, the sequential down-regulation and up-regulation by PGE_2 may serve some physiological role, possibly related to temporal patterning of sensory input.

There are several possible underlying mechanisms at the channel level by which PGE_2 could up-regulate the TTX-s Na^+ current in type-4 DRG cells. These include an increase in unitary conductance, insertion of additional channels into the membrane, a positive shift in the voltage-dependency of channel steady state inactivation, and a negative shift in the voltage-dependency of channel activation. To address this question we demonstrated that PGE_2 and forskolin can increase TTX-s Na^+ current amplitude without affecting V_h. Also, both PGE_2 and forskolin induced a larger percent increase in conductance at weak TPs versus strong TPs. Finally, the modeling study suggested that PGE_2 and forskolin both induced changes in channel gating. Each of these three lines of experimentation argue against an increase in channel number or unitary conductance as the sole underlying mechanisms. Also, simulations depicted in Fig 7D, E, and F indicate that increases in channel number or unitary conductance would result in control and up-regulated current records that do not differ regarding macroscopic activation and inactivation rates. This scenario does not match with our analysis of simulations presented in Fig. 7B and C, suggesting that both PGE_2 and forskolin do induce significant changes in macroscopic activation and inactivation rates.

The I-V data acquired yielded some contradictory results regarding the question of whether PGE_2 or forskolin altered the voltage-dependency of channel activation. After correction for drift observed in untreated controls over the same period of time between I-Vs, the average negative shift in V_a associated with both PGE_2 and forskolin induced up-regulation was small, and up-regulation by both agents was observed in cases where there was a positive shift in V_a. On the other hand, both PGE_2 and forskolin induced a significantly larger proportional increase in current amplitude for currents evoked by more negative TPs around −30 mV compared to currents evoked by more positive TPs around 10 mV. It can be argued that this pattern fits the definition of “voltage-dependent”. Regardless of nomenclature, the pattern of modulation of current amplitude versus voltage observed for PGE_2 and forskolin could serve an important physiological role. The corrected PGE_2 I-V data indicates that Na^+ current evoked by a TP to −30 mV would be increased by an average of 144 pA after exposure to PGE_2. A previous study found that type-4 DRG cells have an average resting input resistance ≈ 300 MΩ (Cardenas et al., 1995). If the peripheral sensory receptors of type-4 DRG neurons resemble their cell bodies regarding input resistance, a generator potential that would normally peak at −30 mV, could possibly result in an additional 40 mV of depolarization due to augmentation of Na^+ influx by PGE_2. Outward K^+ currents in type-4 DRG cells, evoked by TPs to −30 mV are relatively small and slow (R. Scroggs, unpublished observations). Thus the augmentation of Na^+ currents by PGE_2 near voltages where action potentials are initiated could be largely unopposed and greatly boost excitability. On the other hand, the proportionally lower increases in current amplitude

induced by PGE_2 at more positive voltages could serve to strengthen signaling by reducing action potential failure rate during high frequency firing. The present study does not rule out the possibility that the disproportional effect of PGE_2 and forskolin on TTX-s current at weak versus strong TPs results from the differential modulation of multiple splice variants or isoforms of TTX-s Na^+ channels that may be expressed by type-4 DRG cells, similar to the case reported for splice variants of $Na_V1.7$ channels expressed by human sensory neurons (Chatelier et al,,2008)

The Markov model employed in the modeling studies presented here is consistent with established typical biophysical properties of TTX-s Na^+ channels, including voltage-dependent transitions through the resting states, voltage-independent opening from the resting state, and voltage-independent inactivation from resting states and the open state (Kuo and Bean, 1994; Patlak, 1991; Vandenberg and Bezanilla, 1991). Estimates of rate constants obtained by fitting the current records with the model provide some insights regarding how PGE_2 and forskolin increase peak Na^+ conductance, and why forskolin produced a significantly greater increase of TTX-s current than PGE_2. The results of the modeling experiments suggest that both PGE_2 and forskolin increase the rate of channel opening, which would tend to increase open probability and peak conductance. However, the modeling suggests that forskolin has an additional effect of increasing the rate of forward transitions through the resting states, which could allow forskolin to induce larger increases in open probability and peak current amplitude than PGE_2. In addition, PGE_2 but not forskolin, significantly increased the voltage-dependency parameter VDBack, which simulations indicate would oppose other effects of PGE_2 on channel gating that tend to increase peak TTX-s Na^+ current. This latter putative effect of PGE_2 on channel gating could also explain, in part, why PGE_2 produced smaller increases in TTX-s Na^+ current amplitude than forskolin. In addition it may explain why PGE_2 produced significantly larger decreases in TTX-s Na^+ current amplitude than forskolin, when the two agents were applied in the presence of Rp-cAMPs. Possibly, PGE_2 activates two signaling pathways; a PKA-dependent pathway, which couples in an overall positive way to TTX-s Na^+ channels in type-4 DRG cells, and another, such as a PKC-dependent pathway, which couples to these TTX-s channels in a primarily negative way. This putative second signaling pathway could possibly mediate the PGE_2 induced increases in VDBack.

As outlined in the introduction, the role(s) played by sensory neurons with type-4 cell bodies in sensory transmission is not clearly understood. On the one hand, there is indirect evidence that type-4 DRG cells may represent non-nociceptive low-threshold D-hair mechanoreceptors, while on the other, type-4 DRG cells have been shown to express several properties usually attributed to nociceptors. If type-4 DRG cells represent some type of nociceptor, then possibly the modulation of TTX-s channels by inflammatory mediators in these neurons could play a role in hyperalgesia, allodynia, and neuropathic pain. On the other hand, if type-4 DRG cells represent D-hair receptors, it is unclear what physiological role modulation of TTX-s channels by PGE_2 would play. To our knowledge, the modulation of TTX-s channels by inflammatory mediators in a non-nociceptive afferent has never before been reported. However, we have shown here that TTX-s Na^+ channels in type-4 DRG cells are modulated by the inflammatory mediator PGE_2. Also, in a previous report we demonstrated that I_H current in type-4 DRG cells is up-regulated by serotonin via a cAMP-dependent signaling pathway, and that this up-regulation increases the number of spikes generated during a burst of action potentials riding on a T-type-Ca^{2+} channel mediated plateau. Others have shown that nociceptin inhibits T-type Ca^{2+} currents in medium diameter DRG cells that express large T-type Ca^{2+} currents, and that likely analogous DRG cells express GABA-gated chloride currents (Abdulla and Smith, 1997; White, 1990). The apparent ease with which type-4-like DRG cells can be identified will likely lead to more studies, which may eventually unravel an interesting story regarding the modulation of

sensory input by multiple pathways converging on the afferents represented by type-4-like DRG cell bodies.

List of Abbreviations

A-D/D-A	analog to digital/digital to analogue
ATP	adenosine triphosphate
AC	adenylyl cyclase
cAMP	cyclic adenosine monophosphate
DRG	dorsal root ganglion
EGTA	ethylene glycol tetraacetic acid
G	whole cell conductance
g	unitary (single channel) conductance
GTP	guanosine triphosphate
HEPES	4-(2-hydroxyethyl)-1-piperazineethanesulfonic acid
HP	holding potential
MΩ	megaohm
I	whole cell current
i	unitary (single channel) current
PGE_2	prostaglandin E_2
PKA	Protein Kinase A
PKC	Protein Kinase C
TEA	tetraethylammonium chloride
TEA-OH	tetraethylammonium hydroxide
TP	test potential
TTX	tetrodotoxin

Acknowledgments

This research was supported by National Institutes of Health (NIH), Research Grant NS37067.

References

Abdulla FA, Smith PA. Nociceptin inhibits T-type Ca^{2+} channel current in rat sensory neurons by a G-protein-independent mechanism. J Neurosci. 1997; 17:8721–8728. [PubMed: 9348341]

Abdulla FA, Smith PA. Changes in Na^+ channel currents of rat dorsal root ganglion neurons following axotomy and axotomy-induced autotomy. J Neurophysiol. 2001; 88:2518–2529. [PubMed: 12424291]

Barber MJ, Wendt DJ, Starmer CF, Grant AO. Blockade of cardiac sodium channels: competition between the permeant ion and antiarrhythmic drugs. J Clin Invest. 1992; 90:368–381. [PubMed: 1322937]

Black JA, Liu S, Tanaka M, Cummins TR, Waxman SG. Changes in the expression of tetrodotoxin-sensitive sodium channels within dorsal root ganglia neurons in inflammatory pain. Pain. 2004; 108:237–247. [PubMed: 15030943]

Bley KR, Hunter JC, Eglen RM, Smith JAM. The role of IP prostanoid receptors in inflammatory pain. TiPS. 1998; 19:141–147. [PubMed: 9612089]

Carbone E, Swandulla D. Neuronal calcium channels: kinetics, blockade, and modulation. Prog Biophys molec Biol. 1989; 54:31–58. [PubMed: 2577439]

Cantrell AR, Ma JY, Scheuer T, Catterall WA. Muscarinic modulation of sodium current by activation of protein kinase C in rat hippocampal neurons. Neuron. 1996; 16:1019–1026. [PubMed: 8630240]

Cantrell AR, Smith RD, Goldin AL, Scheuer T, Catterall WA. Dopaminergic modulation of sodium current in hippocampal neurons via cAMP-dependent phosphorylation of specific sites in the sodium channel α subunit. J. Neurosci. 1997; 17:7330–7338. [PubMed: 9295379]

Cardenas CA, Scroggs RS. Prostaglandin E_2 increases TTX-sensitive sodium current in rat aδhigh-threshold mechanoreceptors. Society for Neuroscience Abstracts. 2003 #380.7.

Cardenas CG, Del Mar LP, Scroggs RS. Variation of serotonergic inhibition of calcium channel currents in four types of rat sensory neurons differentiated by membrane properties. J. Neurophysiol. 1995; 74:1870–1879. [PubMed: 8592180]

Cardenas CG, Del Mar LP, Cooper BY, Scroggs RS. $5HT_4$ receptors couple positively to tetrodotoxin-insensitive sodium channels in a subpopulation of capsaicin sensitive rat sensory neurons. J Neurosci. 1997; 17:7181–7189. [PubMed: 9295364]

Cardenas CG, Del Mar LP, Vysokanov A, Arnold PB, Cardenas LM, Surmeier DJ, Scroggs RS. Sertonergic modulation of hyperpolarization-activated currents in acutely isolated rat dorsal root ganglion cells. J Physiol. 1999; 518:507–523. [PubMed: 10381596]

Caterina MJ, Julius D. The vanilloid receptor: a molecular gateway to the pain pathway. Annu Rev Neurosci. 2001; 24:487–517. [PubMed: 11283319]

Chatelier A, Dahllund L, Eriksson A, Krupp J, Chahine M. Biophysical properties of human $Na_V1.7$ splice variants and their regulation by PKA. J Neurophysiol. 2008; 99:2241–2250. [PubMed: 18337362]

Coste B, Crest M, Delmas P. Pharmacological dissection and distribution of NaN/$Na_V1.9$, T-type Ca^{2+} currents, and mechanically activated cation currents in different populations of DRG neurons. J Gen Physiol. 2007; 129:57–77. [PubMed: 17190903]

Docherty RJ, Farrag KJ. The effect of dibutyryl cAMP on tetrodotoxin-sensitive and –resistant voltage-gated sodium currents in rat dorsal root ganglion neurons and the consequences for their sensitivity to lidocaine. Neuropharmacol. 2006; 51:1047–1057.

Dubreuil AS, Boukhaddaoui H, Desmadryl G, Martinez-Salgado C, Moshourab R, Lewin GR, Carroll P, Valmier J, Scamps F. Role of T-type calcium current in identified D-hair mechanoreceptor neurons studied *in vitro*. J Neurosci. 2004; 24:8480–8484. [PubMed: 15456821]

Fang X, McMullan S, Lawson SN, Djouhri L. Electrophysiological differences between nociceptive and non-nociceptive dorsal root ganglion neurones in the rat *in vivo*. J Physiol. 2005; 565.3:927–943. [PubMed: 15831536]

Gold MS, Levine JD, Correa AM. Modulation of TTX-r I_{Na} by PKC and PKA and their role in PGE_2-induced sensitization of rat sensory neurons *in vitro*. J Neurosci. 1998; 18:10345–10355. [PubMed: 9852572]

Kuo CC, Bean BP. Na^+ channels must deactivate to recover from inactivation. Neuron. 1994b; 12:819–829. [PubMed: 8161454]

Li M, West JW, Lai Y, Scheuer T, Catterall WA. Functional modulation of brain sodium channels by cAMP-dependent phosphorylation. Neuron. 1992; 8:1151–1159. [PubMed: 1319185]

Milescu LS, Akk G, Sachs F. Maximum likelihood estimation of ion channel kinetics from macroscopic currents. Biophys. J. 2005; 88:2494–2515. [PubMed: 15681642]

Nelson MT, Milescu LS, Todorovic SM, Scroggs RS. A modeling study of T-type Ca^{2+} channel gating and modulation by L-cysteine in rat nociceptors. Biophysical Journal. 2010; 98:197–206. [PubMed: 20338841]

Patlak J. Molecular kinetics of voltage -dependent Na^+ channels. Physiological Reviews. 1991; 71:1047–1080. [PubMed: 1656476]

Petruska JC, Napaporn J, Johnson RD, Gu JG, Cooper BY. Subclassified acutely dissociated cells of rat DRG: histochemistry and patterns of capsaicin-, proton, and ATP-activated currents. J Neurophysiol. 2000; 84:2365–2379. [PubMed: 11067979]

Scroggs RS, Fox AP. Calcium current variation between acutely isolated adult rat dorsal root ganglion neurons of different size. J Physiol. 1992a; 445:639–658. [PubMed: 1323671]

Scroggs RS, Fox AP. Multiple Ca^{2+} currents elicited by action potential waveforms in acutely isolated adult rat dorsal root ganglion neurons. J Neurosci. 1992b; 12:1789–1801. [PubMed: 1578270]

Scroggs RS, Todorovic S, Anderson EG, Fox AP. Variation in I_H, I_{IR}, and I_{LEAK} between acutely isolated rat dorsal root ganglion neurons of different size. J Neurophysiol. 1994; 71:271–279. [PubMed: 7512627]

Shin JB, Martinez-Salgado C, Heppenstall PA, Lewin GR. A T-type calcium channel required for normal function of a mammalian mechanoreceptor. Nature Neuroscience. 2003; 6:724–730.

Smith RD, Goldin AL. Potentiation of rat brain sodium channel currents by PKA in Xenopus oocytes involves the I–II linker. Am J Physiol Cell Physiol. 2000; 278:C638–C645. [PubMed: 10751312]

Vandenberg CA, Bezanilla F. A sodium channel gating model based on single channel macroscopic ionic, and gating currents in the squid giant axon. Biophys J. 1991; 60:1511–1533. [PubMed: 1663796]

White G. GABA-receptor-activated current in dorsal root ganglion neurons freshly isolated from adult rats. J Neurophysiol. 1990; 64:57–63. [PubMed: 2167353]

White G, Lovinger DM, Weight FF. Transient low-threshold Ca^{2+} current triggers burst firing through an afterdepolarizing potential in adult mammalian neuron. Proc Natl Acad Sci USA. 1989; 86:6802–6806. [PubMed: 2549548]

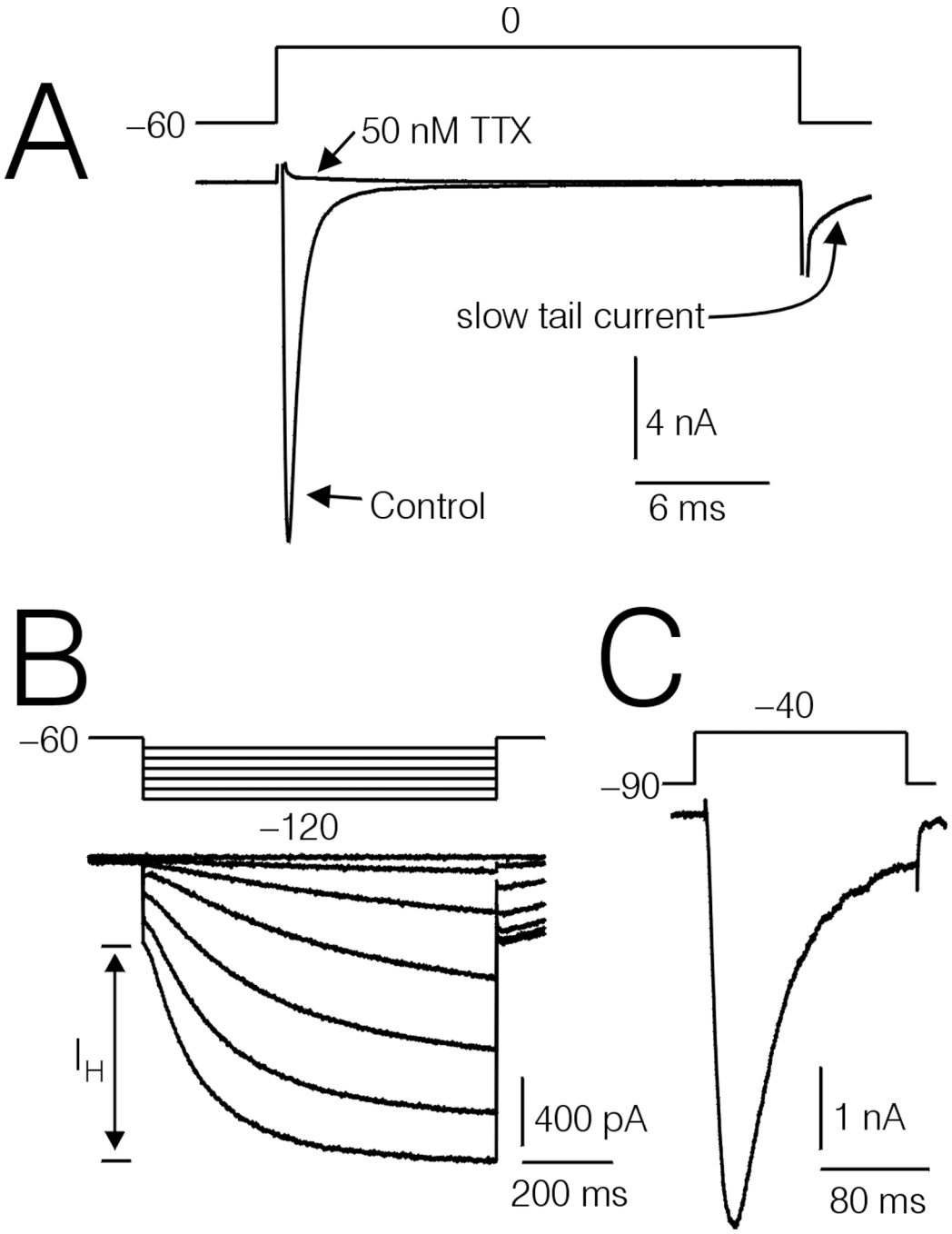

Figure 1.

Several prominent characteristics of type-4 DRG cells. A, Na^+ currents recorded under control conditions, and after treatment with 50 nM TTX. Note the slow tail current (arrow) probably resulting from unblock of T-type Ca^{2+} channels by Cd^{2+} upon returning the cell interior to −90 mV. B, Large I_H currents (slow inward component evoked by hyperpolarizations to −70 through −120 mV from a holding potential of −60 mV). C, Large T-type Ca^{2+} currents, recorded in an external solution containing 140 mM TEA and 2 mM $BaCl_2$.

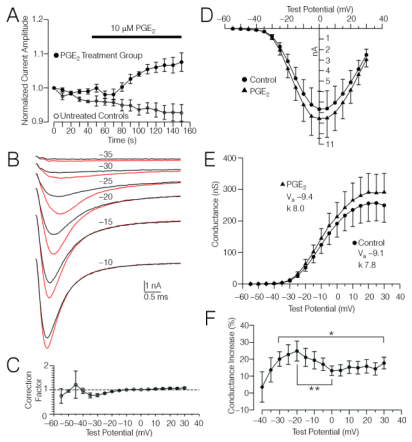

Figure 2.

Effects of PGE_2 on Na^+ currents in type 4 DRG cells. A, Plot of normalized amplitude of Na^+ currents evoked by test potentials (TP) to −10 mV versus time for 7 type-4 DRG cells tested with PGE_2 (filled circles), and for 4 untreated control type-4 DRG cells (open circles). The data were normalized relative to the amplitude of the first current in each series shown. The time course of PGE_2 treatment (10 μM) is indicated by the horizontal bar. B, Averaged current records acquired from the 7 type-4 DRG cells depicted in (A) evoked by TPs ranging from −35 mV to −10, under control conditions (black traces) and after PGE_2 treatment (red traces). C, Correction factors derived from comparisons of current-voltage (I-V) data acquired from the untreated controls depicted in (A) before and after an average of 213 sec (see Experimental Procedures). D, Corrected I-V data acquired from the 7 type-4 DRG cells depicted in (B) before and after PGE_2 treatment. The I-V data was extrapolated for the TPs shown from I-V plots where TPs were adjusted for voltage error caused by Rs, and then corrected for spontaneous drift observed in the untreated controls using the average correction factors shown in (C). E, Conductance-voltage (G-V) relationship calculated from the data shown in (D). Insets show the values for V_a and k before and after PGE_2 treatment, derived by fitting normalized G-V curves (corrected data) with a Boltzmann function as described in Experimental Procedures. The reversal potentials for the 7 DRG cells averaged 40.7 ± 1.3 mV and 40.5 ± 1.2 mV, respectively, before and after PGE_2 treatment. F, Plot of the percent increase in conductance versus TP, calculated from the data shown in (D). * Significant change in percent increase in conductance over the range of TPs indicated by the bracket (Friedman-test, $p < 0.05$). ** Significant decrease in percent increase in conductance at ≈0 mV versus that observed at ≈−20 mV ($p < 0.05$, Wilcoxon test).

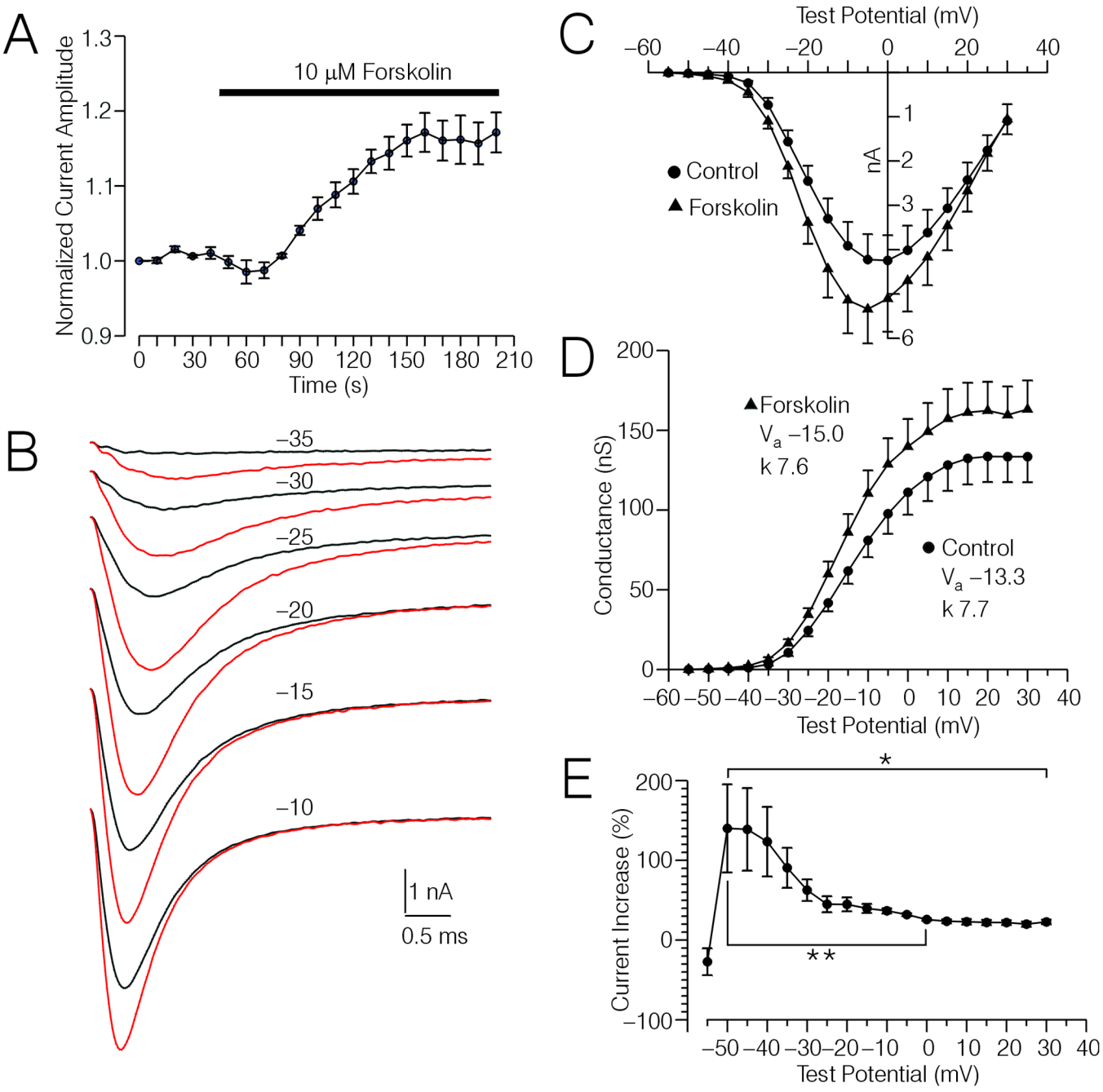

Figure 3.

Effects of forskolin on Na^+ currents in type-4 DRG cells. A, Plot of Na^+ current amplitude versus time for 6 type-4 DRG cells. The time course of forskolin treatment (10 μM) is indicated by the horizontal bar. B, Averaged current records acquired from the 6 type-4 DRG cells depicted in (A) evoked by test potentials (TP) ranging from −35 mV to −10, under control conditions (black traces) and after forskolin treatment (red traces). C, I-V relationship of the Na^+ current recorded from the 6 type-4 DRG cells depicted in (B) before and after forskolin treatment. The data points were extrapolated and corrected for spontaneous drift in the same manner as for the PGE_2 data depicted in Fig 2D. D, G-V relationship calculated from the data shown in (C). insets show the values for V_a and k

before and after forskolin treatment. These values were obtained by fitting normalized G-V curves (corrected data) with a Boltzmann function as described in Experimental Procedures. The reversal potentials for the 6 DRG cells averaged 38.2 ± 2.0 mV and 36.2 ± 1.7 mV, respectively before and after forskolin treatment. E, Plot of the percent increase in conductance versus TP, calculated from the data shown in (C). * Significant change in percent increase in conductance over the range of TPs indicated by the bracket (Friedman-test, $p < 0.05$). ** Significant decrease in percent increase in conductance at ≈0 mV versus that observed at ≈−50 mV ($p < 0.05$, Wilcoxon test).

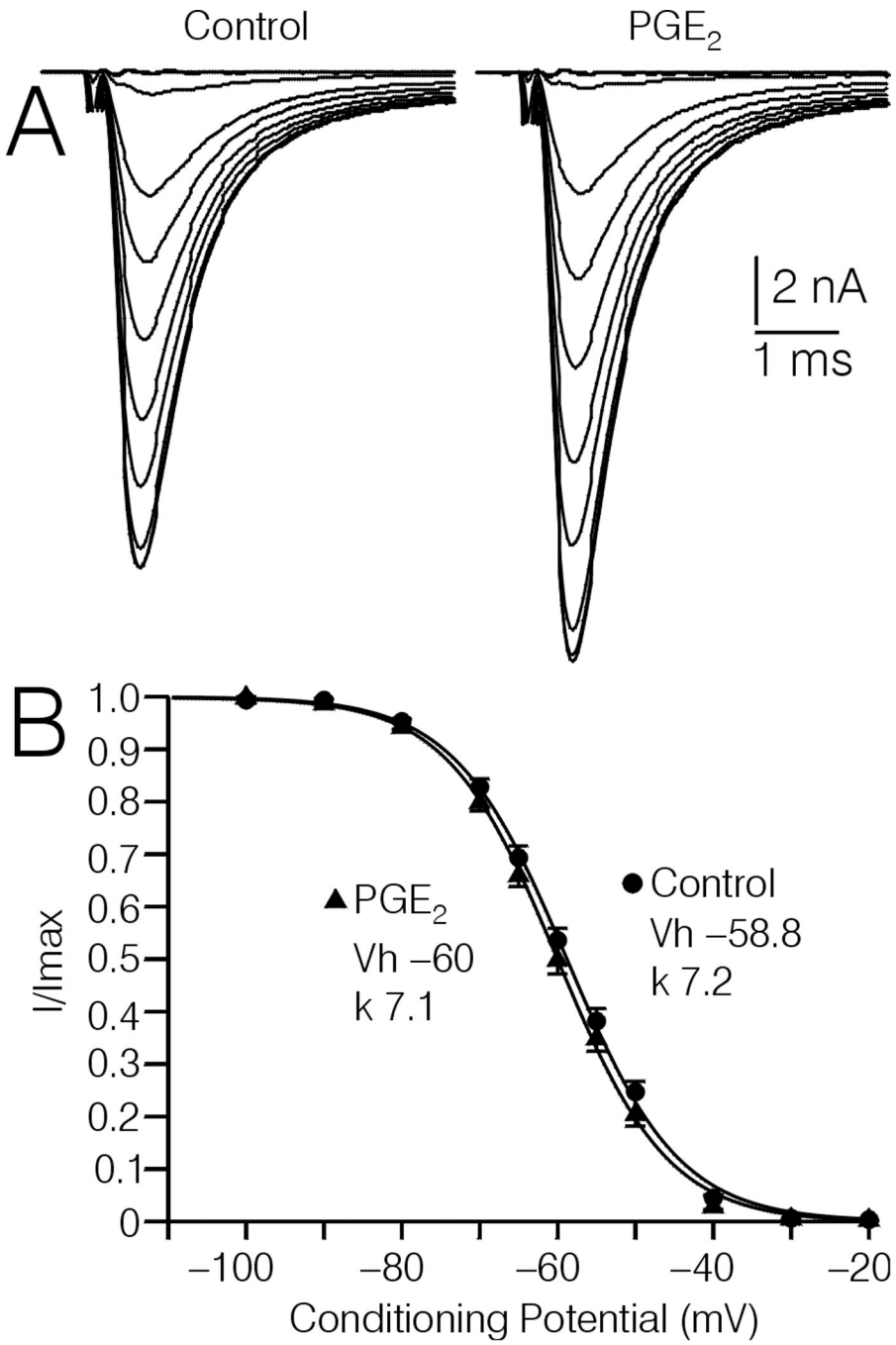

Figure 4.

Effect of PGE_2 on steady state inactivation of Na^+ currents recorded from type-4 DRG cells. A, Averaged current traces acquired from 5 type-4 DRG cells following 500 ms conditioning pulses to −100 to −20 mV, before and after treatment with 10 μM PGE_2. B, Plot of I/Imax versus voltage for the 5 DRG cells depicted in (A). Inset, average values of V_h, and k obtained by fitting individual plots of I/Imax versus voltage with a Boltzmann function as described in Experimental Procedures. The lines through the data points in (B) were drawn according to the average values shown in the insets.

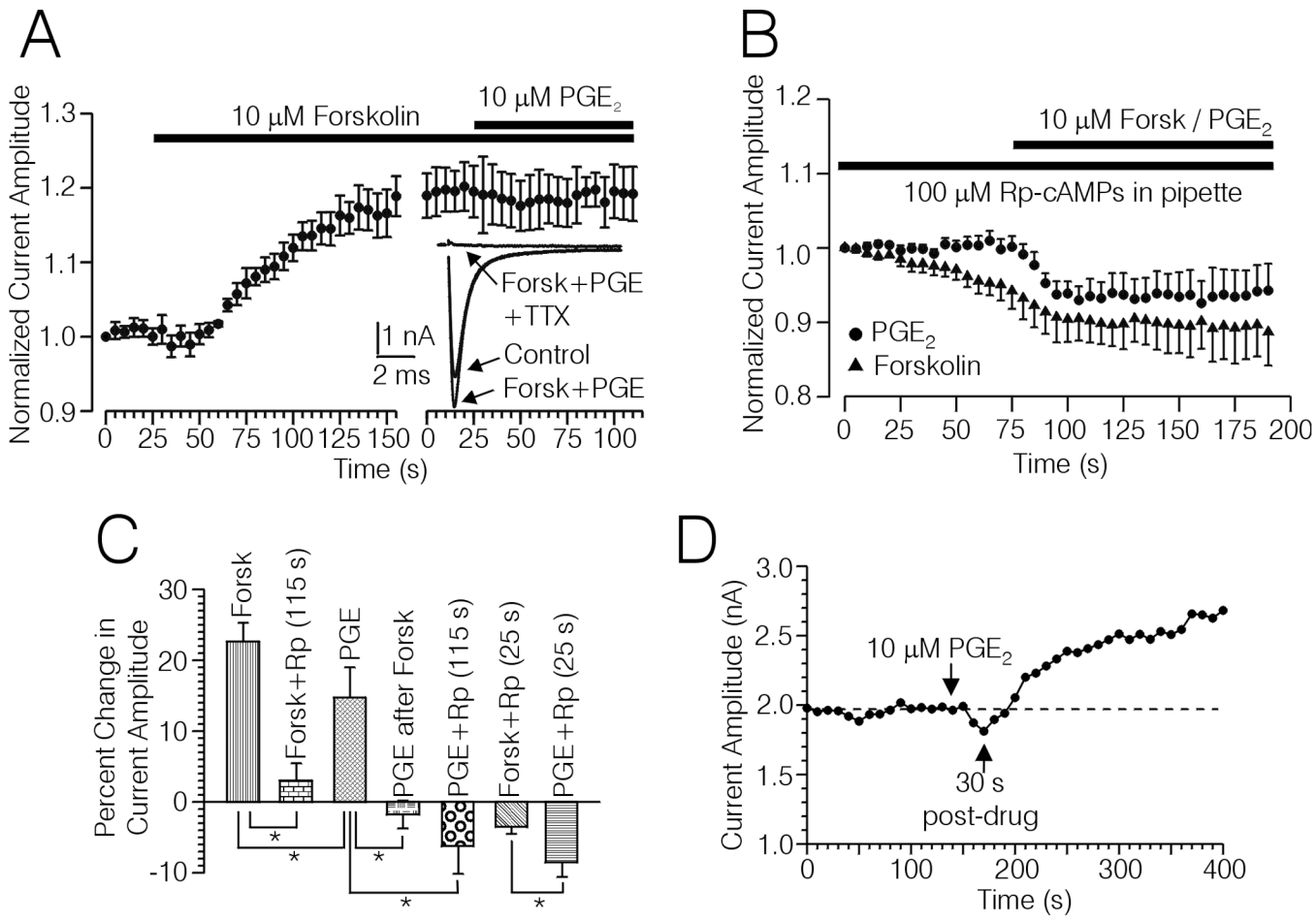

Figure 5.

Occlusion of the effects of PGE_2 with forskolin, and block by TTX and Rp-cAMPs of the PGE_2 and forskolin induced up-regulation of Na^+ current. A, Plot of Na^+ current amplitude versus time recorded from 5 type-4 DRG cells. The horizontal bars indicate the duration of treatment with forskolin (10 μM), and forskolin + 10 μM PGE_2. Inset, Averaged current records acquired from the plot shown in (A) after treatment with forskolin and PGE_2, and following treatment with 50 nM TTX in the presence of forskolin and PGE_2. B, Plot of Na^+ current versus time acquired from type-4 DRG cells recorded from with 100 μM Rp-cAMPs included in the pipette and treated with PGE_2 (n = 7, filled circles) or forskolin (n = 10, filled triangles). The horizontal bar indicates the duration of treatment with 10 μM forskolin or PGE_2. C, Bargraph summarizing the effects of PGE_2 and forskolin on Na^+ currents evoked with TPs to −10 mV from type-4 DRG cells under various conditions; in the absence of Rp-cAMPs (PGE, n = 12, Forsk, n = 12), PGE_2 following up-regulation of Na^+ current with forskolin (PGE after Forsk, n = 5), in the presence of Rp-cAMPs after an average of ≈ 25 sec following initiation of drug treatment (PGE + Rp (25 s), n = 7), (Forsk + Rp (25s), n = 10), and at the end of the plot (PGE + Rp (115 s), n = 7), Forsk + Rp (115 s), n = 10. * significant difference between the means indicated by each bracket, ($p < 0.05$, Mann Whitney U-test). In cases where a mean is compared multiple times the α-level has been adjusted using the Bonferroni adjustment for multiple comparisons. D, Example of a biphasic response of a type-4 DRG cell regarding PGE_2 induced changes in the amplitude of Na^+ current evoked with TPs to −10 mV in the absence of Rp-cAMPs.

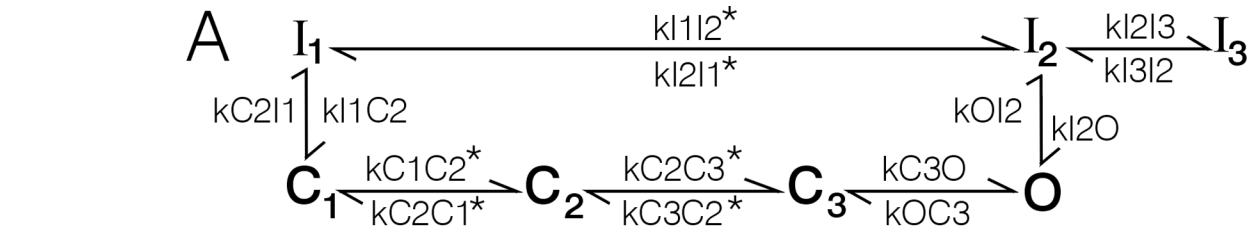

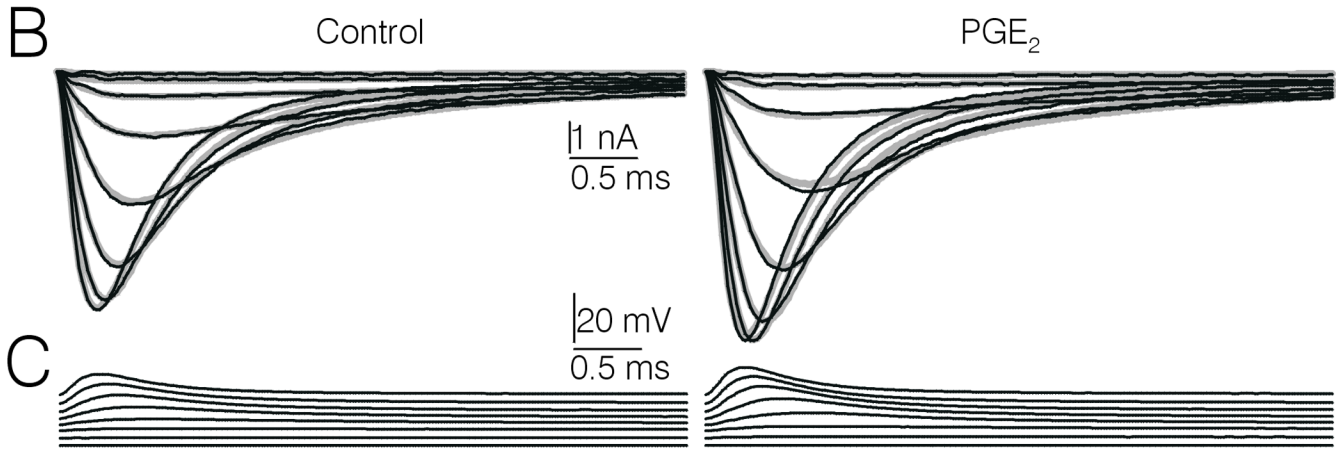

D

	kC1C2	kC2C3	kC3O	kC1I1	kI2I3	VDBack
Con 1	153039 ± 18590	29723 ± 3611	4964 ±168	279 ± 49	207 ± 42	−0.0405 ± 0.0028
PGE_2	122323 ± 7156	23757 ± 1390	6369 ±647	338 ± 66	337 ± 53	−0.0650 ± 0.0040
Prob	n.s.	n.s.	0.028	n.s.	0.043	0.028
Con 2	120267 ± 19344	23358 ± 3757	4567 ±273	693 ± 213	194 ± 49	−0.0517 ± 0.0095
Forsk	177458 ± 34002	34465 ± 6604	6160 ±513	588 ± 167	329 ± 40	−0.0519 ± 0.0126
Prob	0.028	0.028	0.028	0.046	n.s.	n.s.

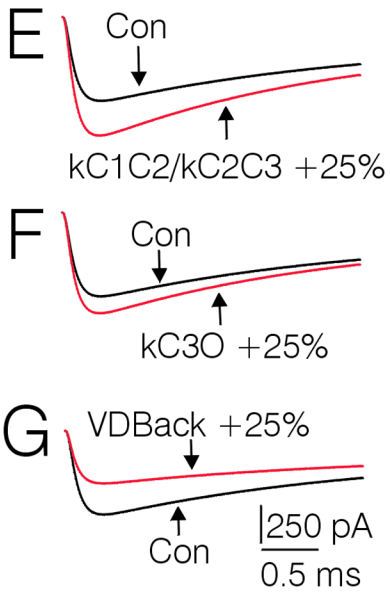

Figure 6.

Generation of kinetic rate constants corresponding to control and PGE_2 and forskolin treatment by fitting a Markov channel state model to type-4 DRG cell Na^+ current records. A, Markov model used to fit current records. kC1C2, kC3O, kC1I1, kOI2, kI2O, kC2C3, kI2I3, and the voltage-dependence parameters for kC1C2 and kC3C2 were set free. kC2C3 was scaled to kC1C2 at a ratio of ≈ 1:5. KC2C1 was scaled equal to kC3C2. kI1C1 was scaled with kC1I1 at a ratio of 1:10. KI1I2 was scaled to kC1I1 at a ratio of 150:1 at 0 mV. The voltage-dependence terms in the forward direction were scaled to be equal, as were the voltage-dependence terms in the backward direction. kOC3 and kI3I2 were fixed at 2000/sec and 1/sec, respectively. The rate constants that were set voltage-dependent are marked with

an asterisk. The rate constants and voltage-dependence terms in the model were loop balanced so that the product of the forward rate constants equaled the product of the backward rate constants. B, Real currents averaged from 7 type-4 DRG cells before and after treatment with PGE_2 (thin black lines), superimposed on simulated currents drawn according to the corresponding sets of parameters arrived at during fitting (thick gray lines). C, plot of the voltage files (adjusted for R_s) used by MAC to fit the model to the data. D, Table showing the average kinetic rate constants and voltage-dependence terms obtained by fitting the model to individual sets of currents records corresponding to PGE_2 and forskolin treatment conditions and their respective pretreatment controls. Only the parameters that were significantly affected by PGE_2 or forskolin are included. The control parameters correspond to fits to real currents. The parameters for PGE_2 and forskolin treatment conditions were obtained by fitting simulated current records that had been corrected for spontaneous drift in gating properties observed in untreated controls, using the correction records depicted in Fig. 7A. The rate constants are expressed as transitions^{sec-1}. The voltage-dependence terms are expressed as mV^{-1}. Where a significant change in a given rate constant following PGE_2 or forskolin was detected, the probability is shown below. n.s. stands for not significant. The parameters kC1C2 and kC2C3 were scaled, thus the statistical analysis was actually only performed on kC1C2. The Wilcoxon-test was used for all comparisons. E, F, and G, Simulations showing the effects of changing one parameter at a time on Na^+ current amplitude and macroscopic activation and inactivation rate. The black lines represent control conditions and the red lines represent the current after the indicated rate constants have been changed by 25%.

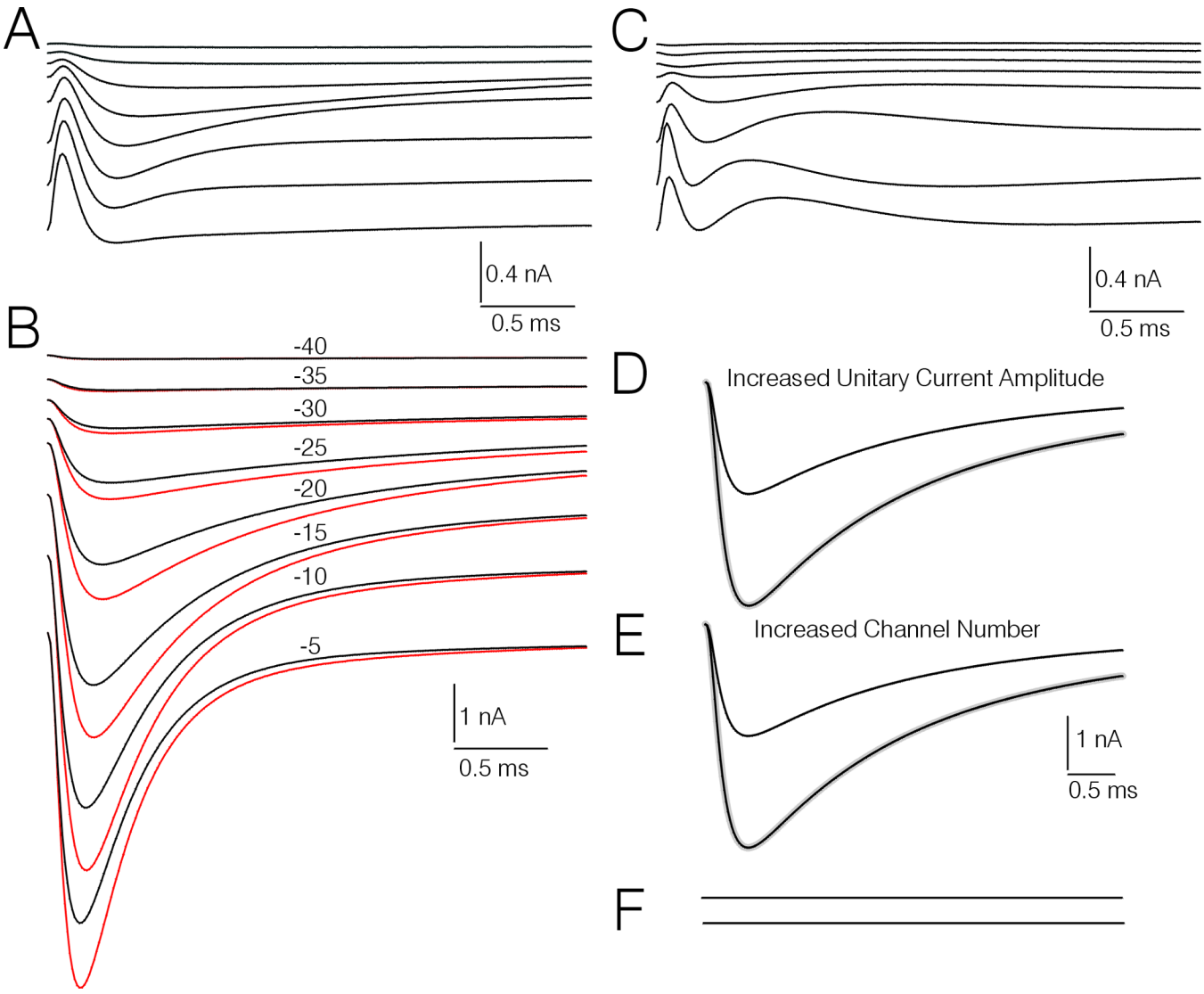

Figure 7.

Comparison of the peak amplitude, and macroscopic activation and inactivation rates of simulated currents corresponding to control and PGE_2 treatment. A, averaged difference currents obtained by subtracting simulated untreated control records corresponding to real records evoked by TPs to −40 mV through −5 mV before and after a 213 sec interval. B, Simulated current records corresponding to PGE_2 treatment (red traces) and pre-drug controls (black traces) evoked by TPs to −40 mV through −5 mV. The simulated records corresponding to PGE_2 treatment have been corrected for spontaneous drift occurring in the untreated control DRG cells by subtracting appropriately scaled versions of the difference currents shown in (A). The numbers above each of traces indicate the TP. C, Difference records generated by subtracting the pairs of simulated control and PGE_2 treatment currents corresponding to equivalent TPs in (B). D and E, Simulations of increased current amplitude resulting from increased unitary conductance (D), or increased number of channels (E). Each of the smaller amplitude black traces represent control simulated currents evoked by a TP to −20 mV in a neuron with 45,888 channels that have a unitary current amplitude of −0.6 pA. The larger amplitude black traces represent a second simulated record where the unitary current amplitude is doubled (D) or the channel number is doubled (E). The gray

traces represent the control traces scaled up at their peaks to match the traces where unitary conductance or channel number is doubled. F, Difference records obtained by subtracting the scaled up control records from the records representing increased unitary conductance or increased channel number.